www.ietdl.org

Published in IET Power Electronics
Received on 9th March 2012
Revised on 21st July 2012
doi: 10.1049/iet-pel.2012.0115

ISSN 1755-4535

# Experimental examination on a new switched reluctance wind power generator system for electric vehicles

*Y.J. Bao K.W.E. Cheng N.C. Cheung S.L. Ho*

*Electrical Engineering, The Hong Kong Polytechnic University, Hong Kong*
*E-mail: eeecheng@polyu.edu.hk*

**Abstract:** Renewable energy sources require power electronics for the power processing in order to enhance the operation and performance. In this study, a method of harnessing wind power on-board of an electric vehicle using switched reluctance generator (SRG) coupled to a wind turbine, which is mounted on the vehicle is discussed. The wind turbine integrated with SRG poses a number of challenges for vehicle application as the location and the design are special. The present investigation aims at acquiring the first hand experience in the practical implementation of such a system for on-board power generation. Various configurations of wind turbines are studied. The experimental test from a prototype is presented to validate the theoretical predictions.

## 1 Introduction

Electric vehicles (EVs) and hybrid electric vehicles (HEVs) show very encouraging results in cutting down the pollution [1, 2]. The immature of charging infrastructure and considerable charging time are part of the reasons for the slow acceptance of pure EVs in public. Other alternative sources such as solar, fuel cells and wind have been used in conjunction with the primary battery source. The advantage of the alternative solutions is that the power can be generated on-board even when the vehicle is stationary thus permitting the usage of luxury loads. The concept of on-board power generation to drive certain loads when the engine is switched may become an integral part of any vehicular electrical design in the future because of environmental issues. The other advantage of on-board power generation using alternative sources is that the batteries can be charged while the vehicle is in motion thus reducing the reliance on the charging station.

Fuel-cells based on-board power generation still needs on-board energy storage for transient changes in the load profiles and under power regeneration. The design challenge is to size and integrate the right amount of energy storage to efficiently perform the important function of storing excess energy and supply the power when required by the load [3]. At present, the cost of the fuel cells and the storage are the challenges yet to be addressed for commercial application.

The application of photovoltaic (PV) cells for on-board power generation is too bulky for automotive application [1]. The concept of harnessing wind power by mounting number of small wind-capturing units on a vehicle is discussed in [4, 5]. However, the concept of having number of small wind turbines is not practical to generate enough power to drive the loads of a modern EV.

The switched reluctance machine owing to its simple robust structure, its inherent temperature insensitive property, no rare earth material, absence of field coils and fault tolerance ability makes one of the ideal choices for wind power generation. The ability to maintain high efficiency at different speeds and the capability to operate under automotive or general environment are the other reasons for the growing interest in the use of switched reluctance machine for wind power generation [6, 7]. Chang and Liaw [8] show a grid-connection system using switched reluctance generator (SRG).

The main objectives of the present investigation are, to develop a laboratory testing platform to simulate the wind power assisted SRG operation so as to charge batteries and to support other vital loads in an EV. The motor in the investigation serves to mimic the operation of a wind turbine. The study will focus on the practical issues including dc-link voltage ripple, switching frequency and balancing switching losses in the design of an integrated system that is suitable for an EV. Different controlling methods of the SRG and their relative merits will be compared and a suitable control strategy will be implemented.

## 2 Structure of the new EV

The current investigation focuses on capturing the wind force in a moving vehicle for generating electrical power on-board using wind turbines mounted on vehicles rather than erected on ground. The power required to overcome air drag is proportional to the cube of the relative velocity and to


© The Institution of Engineering and Technology 2012

overcome the rolling drag is shown by Shimizu *et al* [9]

$$P_R = P_r + P_a = \mu m_t v + \rho C_d S v^3 \quad (1)$$

where $P_r$ and $P_a$ represent the rolling and air drag powers, $\mu$ and $C_d$ are the rolling and air drag coefficients, respectively, which combine with other factors of the vehicle specifications such as total vehicle weight $m_t$ and frontal area $S$, with respect to certain conditions, such as vehicle velocity $v$ and air density $\rho$. For increasing the mileage per charge it is to use a part of the air drag to generate the electric power for charging the batteries of EVs or directly supplying some loads of EVs.

The proposed architecture is shown in Fig. 1. On-board power generation is implemented by integrating wind turbines with a SRG. The dual-voltage architecture [10] is adopted here owing to the advantage of the dual-voltage system in driving high-power and low-power loads. The system is named assisted SRG integrated on-board power generation dual-voltage architecture.

In the EV under development, the wind power is captured by two wind turbines that are coaxially connected to a SRG to generate electrical energy. Fig. 2 shows the circuit for the SRG drive [11]. Two capacitors are used for decoupling. One is for bulk energy and one for high-frequency filtering. The output of the generator is used to charge the batteries or to support other loads. Load range can be extended.

The present investigation aims at acquiring skill of practical implementation of such a switched reluctance wind power generator (SRWPG) system for on-board power generation.

## 3 Mounting locations and wind turbine structure

The mounting location and the structure of wind turbine for on-board power generation have to satisfy several factors for successful integration of the turbine and the SRG. The following factors have to be addressed for such an application:

1. The system should not cause appreciable drag;
2. It should not block the driver's view;
3. It should capture as much wind power as possible;
4. It should not hamper the aesthetic appeal of the vehicle.

The regular wind turbines with fewer blades cannot be mounted because of the large wind span of the blades. On the other hand, if the wind span of the blades is reduced the turbine cannot capture enough wind power. Another option is to use a number of smaller wind turbines mounted at various locations to generate the required electrical power but this option requires many generators and has control and management complexity. In order to overcome the limitations of wind turbines, the unit as shown in Fig. 3*a* is considered for the proposed integration. The parameters of the wind turbine are given in Table 1. The advantage of this preferred structure is the easy coupling of the generator

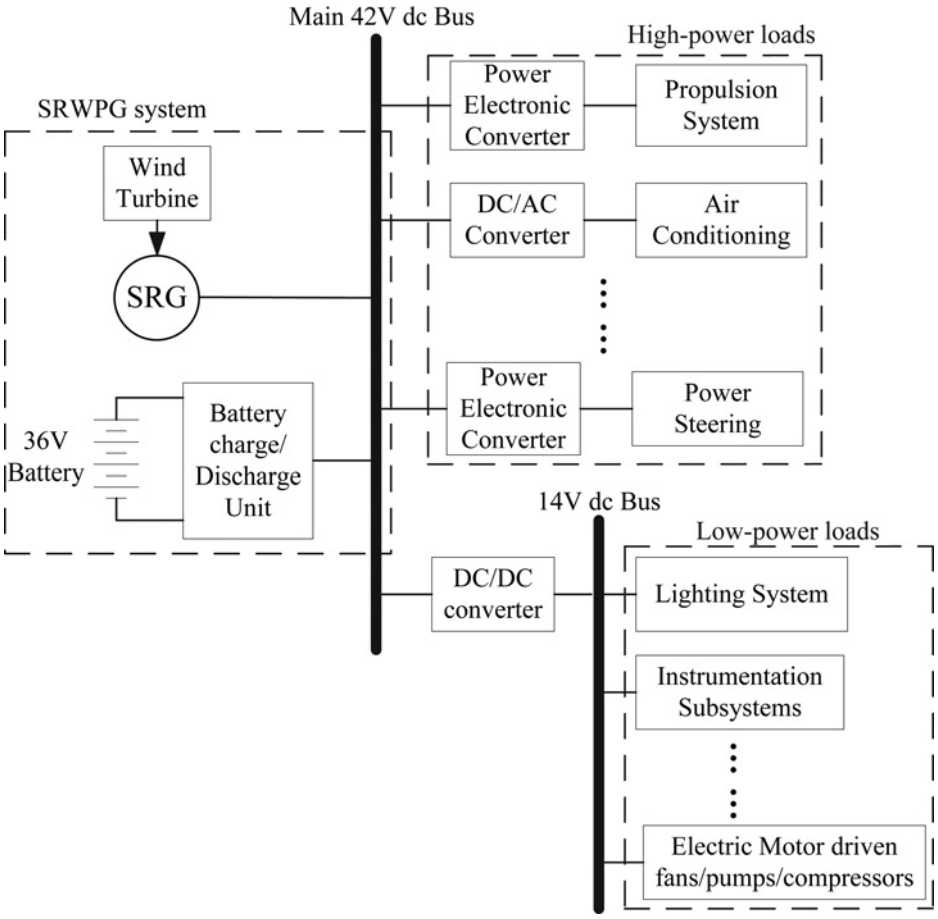


**Fig. 1** *Schematic of a dual-voltage series hybrid architecture using one battery bank*



© The Institution of Engineering and Technology 2012

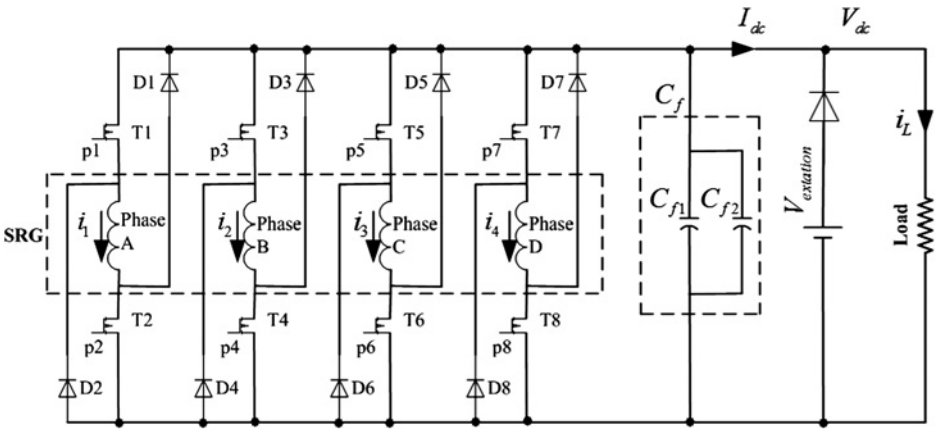


**Fig. 2** *Structure of the power converter (p1–p8, PWM drive signals; T1–T8, IGBTs; D1–D8, power diodes; $i_1$–$i_4$, phase currents; $C_f$, filter capacitors; $I_{dc}$, dc-bus current; $V_{dc}$, dc-bus voltage; i, load current; $V_{excitation}$, excitation voltage)*

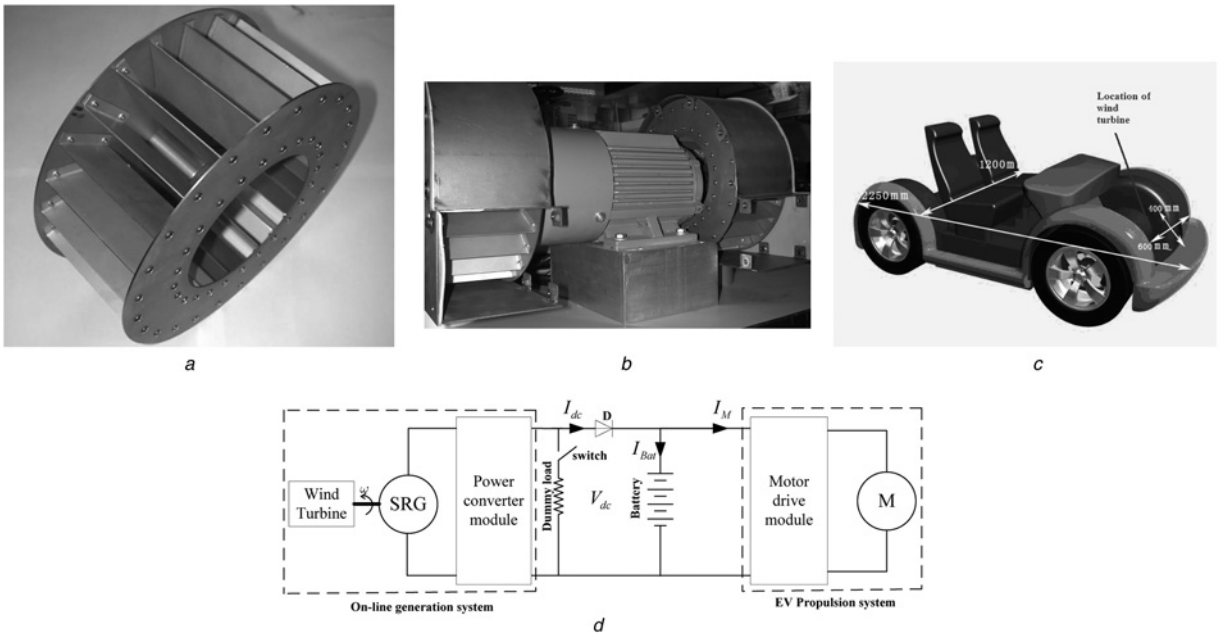


**Fig. 3** *Hardware of the wind turbine system*

*a* Ring wind turbine
*b* Integrated wind turbine
*c* Wind power hybrid EV
*d* Structure of EV with on-board wind generation ($\omega$, angular velocity; $V_{dc}$, dc-bus current; $I_{dc}$, dc-bus current; $I_{Bat}$, battery current; $I_M$, motor drive current; *M*, motor)

with two coaxially mounted wind turbines as shown in Fig. 3*b*.

The wind generator should occupy the main weight of the whole wind generating system. The propulsion motor and batteries are located in the rear and middle parts of the EV. The front of EV is lighter than other parts of the EV and hence the generator is located in the front. The new structure, two coaxially mounted wind turbines coupled with a SRG, can collect energy as much as possible from a moving EV, and can also be conducive to the weight balance of the front of the car body.

**Table 1** Parameters of the wind turbine

| No. | Name | Size, mm |
|---|---|---|
| 1 | length of the blade | 50 |
| 2 | width of the blade | 10 |
| 3 | diameter of the turbine | 250 |
| 4 | diameter of the shaft | 19 |

The scaled drawing of the generator integrated with the ring wind turbines with respect to the EV is shown in Fig. 3*c*. In front of the hood (600 mm × 400 mm), the wind force must exist and may be much larger than that of other locations when a vehicle is moving. The whole structure of EV with on-board wind power generation is shown in Fig. 3*d*. Once the vehicle reaches a certain speed, the wind power captured by wind turbines, will be converted into electric power, which can charge the battery, or directly supply the EV propulsion system. Between the SRG and the battery a power diode *D* is added to avoid the battery current flowing to the SRG. The dummy load is a device used to simulate a load, and in this system, it is for


© The Institution of Engineering and Technology 2012

doi: 10.1049/iet-pel.2012.0115

protecting purposes. In most cases, a switch connected with dummy load is not turned on when under normal operation. When the battery of the EV is fully charged, the switch will be closed, so the generated power will be absorbed by the dummy load in order to keep the whole system safe and simple.

## 4 Proposed control scheme for the SRWPG system

The SRG can be controlled either in constant flux mode [12] or constant power mode [7]. In order to implement constant power control the current as well as the voltage must be sensed, multiplied and compared with the reference power signal. Flux control need dedicated flux model. An improved co-energy control is proposed in [13], but the method is quite complex for practical implementation as it needs a torque sensor and an encoder.

A voltage mode control is used here because the regulated voltage can be directly fed to a battery charge/discharge unit without the need for a separate dc–dc converter interface. The battery charge/discharge unit can transfer the power from the generator to batteries which in turn will feed the power to other loads in the vehicle. Owing to the above reasons the voltage mode control was adopted for this project.

The control system of the SRGs is shown in Fig. 4. $V_{dc}^{*}$ and $I_{ref}$ are the reference dc-link voltage and current, respectively. $\theta_{on}$ and $\theta_{off}$ are turn-on angle and turn-off angle, respectively. $D^{*}$, $i_{ph}$ and $\overline{V_{dc}}$ are the duty ratio, phase current and average dc-bus voltage, respectively. In the proposed work, the well-established proportional-integral (PI) controller is used for the voltage control because of its simplicity instead of more complex control strategies such as iterative learning controller [14] and adaptive controller [15]. PWM and hysteresis controllers that are characterised by their simplicity are proposed to use in current controller. The two current controllers are working alternatively in this system.

## 5 Experimental results setup

A test platform, in which a motor in the investigation serves to mimic the operation of a wind turbine and an electric load (0–100 V/0–60 A) serves to simulate the loads of the EV, is established. Different current controlling methods of the SRG and their relative merits and demerits will be compared and a suitable control strategy has been implemented. The step response performance is verified under constant load and constant speed, and then the dynamic performance is also verified under variable loads or variable speeds.

### 5.1 Test platform

Fig. 5 shows the hardware of the driving circuit and the block diagram representation of the system, respectively. The negative terminal of battery is earthed and is a common path for other electronic circuits in the vehicles. The asymmetrical bridge drivers shown in Fig. 2 are used as the driving circuit for the project. The action of the wind turbine is examined by means of a variable speed switched reluctance motor (SRM) while the load is represented by a resistive load or a battery pack paralleled a resistive load.

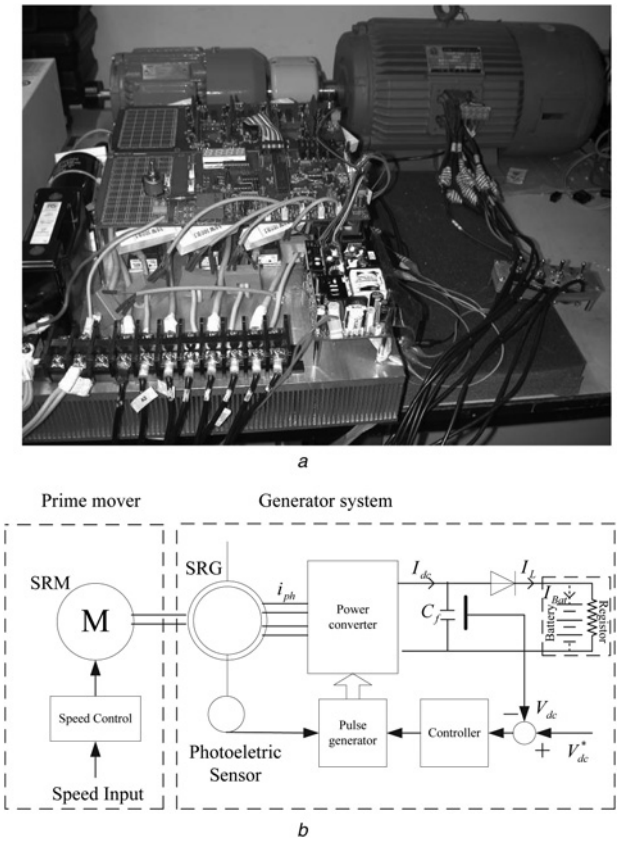


**Fig. 5** *Experimental system*
*a* Photos of experimental system
*b* Block diagram

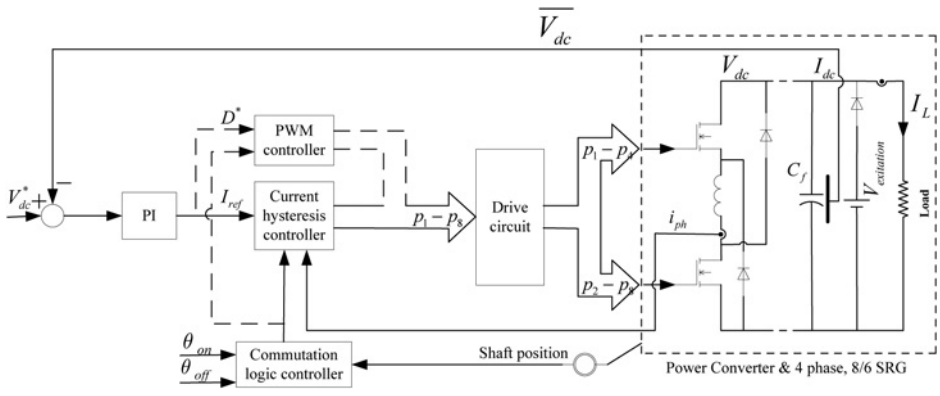


**Fig. 4** *Control structure of the SRG*



© The Institution of Engineering and Technology 2012

The load is assumed to be resistive to simplify the analysis that is always true for such system with a battery and decoupling capacitors. Angular velocity and aligned position are detected by means of photoelectric sensors mounted on stator shaft of the SRG. The system consists of the following key components:

1. Switched-reluctance generator: Four-phase, 8/6, 240 V, 2000 rpm, 5 kW.
2. Driving converter: Classical asymmetric bridge converter is employed (Fig. 2). The switches used in the converter are IGBT modules (FUJI Electric 2MBI-75N-060, 600 V, 75 A).
3. Prime mover: A SRM is utilised to simulate the wind turbine, whose specifications are two-phase SRM: 220 V, 0.55 kW, 1500 rpm.
4. Excitation source: The excitation voltage is to set up the initial flux and 12 V is selected.
5. Control scheme: The control scheme shown in Fig. 4 consists of a closed-loop voltage controller and commutation logic controller. They are realised using the MCU PIC18F4331. The sampling rates are chosen to be 10 kHz for PWM voltage control and 1 kHz for voltage control loop.
6. Some hardware-protecting circuits are adopted, such as over phase current, over line current and over voltage through Hall current sensors, Hall voltage sensors, etc.

### 5.2 Practical aspects

The generated dc-output voltage of an SRG inherently contains significant ripples with dominant ripple frequencies derived from stroke or commutation and PWM switching frequencies. The output voltage ripple can be minimised by choosing proper output filter capacitor. The dc-link voltage $V_{dc}$ can be approximately expressed [16] as

$$V_{dc} = V_0 + \Delta v_{os} + \Delta v_{oh} \tag{2}$$

where $V_0$, $\Delta v_{os}$ and $\Delta v_{oh}$ are average value, stroke ripple component because of phase commutation and PWM ripple component, respectively.

With the consideration of capacitor ESR, the voltage ripple of an SRG $\Delta v_{os}$ can be approximately expressed [16] as

$$\Delta v_{os} \cong V_0 \sqrt{\left(\left(\frac{2R_s}{R_0}\right)^2 + \left(\frac{1}{f_{os}R_0C_f}\right)^2\right)} \tag{3}$$

where $R_s$ is the ESR of $C_f$, $f_{os}$ is the frequency of $\Delta v_{os}$, and $R_0$ is the load resistance.

For the dc-link current $i_d$ with large spikes, the filter should be properly designed to reduce the voltage ripple components $\Delta v_{os}$ and $\Delta v_{oh}$ in (2) through choosing the capacitor with lower ESR at the switching frequency. To achieve this goal, $C_f$ is formed by the parallel connection of a 2200 μF/400 V and 680 μF/400 V. The total value of $C_f$ is determined according to the specified lower-frequency ripple $\Delta v_{os}$. The frequency $f_{os}$ of $\Delta v_{os}$ is directly proportional to the speed, and it is obtained by

$$f_{os} = \frac{S_t 360^\circ}{(360^\circ/((\text{rotor number})(\text{phase number})))60\,\text{s}} = 0.4\,\text{rpm} \tag{4}$$

where $S_t$ is the wind turbine rotational speed in rpm and the motor is 6/4 machine.

Hence, the frequencies $f_{os}$ under $S_t = 250$, 500 and 1000 rpm are 100, 200 and 400 Hz, respectively.

The ESRs of $C_{f1}$, $C_{f2}$ and $C_f$ are measured using Hioki 3532-50 LCR HiTESTER:

$$C_f = C_{f1} + C_{f2} = 2880\,\mu\text{F}$$

where $V_0$, $\Delta v_{os}$, $\Delta v_{oh}$

$R_s$ of $C_{f1}$: 54.07 mΩ/100 Hz, 50.55 mΩ/200 Hz and 48.32 mΩ/400 Hz;
$R_s$ of $C_{f2}$: 71.30 mΩ/100 Hz, 55.61 mΩ/200 Hz and 48.46 mΩ/400 Hz;
$R_s$of $C_f$: 34.88 mΩ/100 Hz, 31.45 mΩ/200 Hz and 29.92 mΩ/400 Hz.

From the above data, it is clear that the ESR of $C_f$ is much smaller than the ESR of $C_{f1}$ in different frequencies, but the equivalent total of $C_f$ is almost determined by the larger capacitor $C_{f1}$ as the capacitance of the capacitor $C_{f2}$ is smaller than that of $C_{f1}$. In other words, it is simply to add additional capacitance in parallel with $C_{f1}$ to reduce $\Delta v_{os}$ as shown in (3).

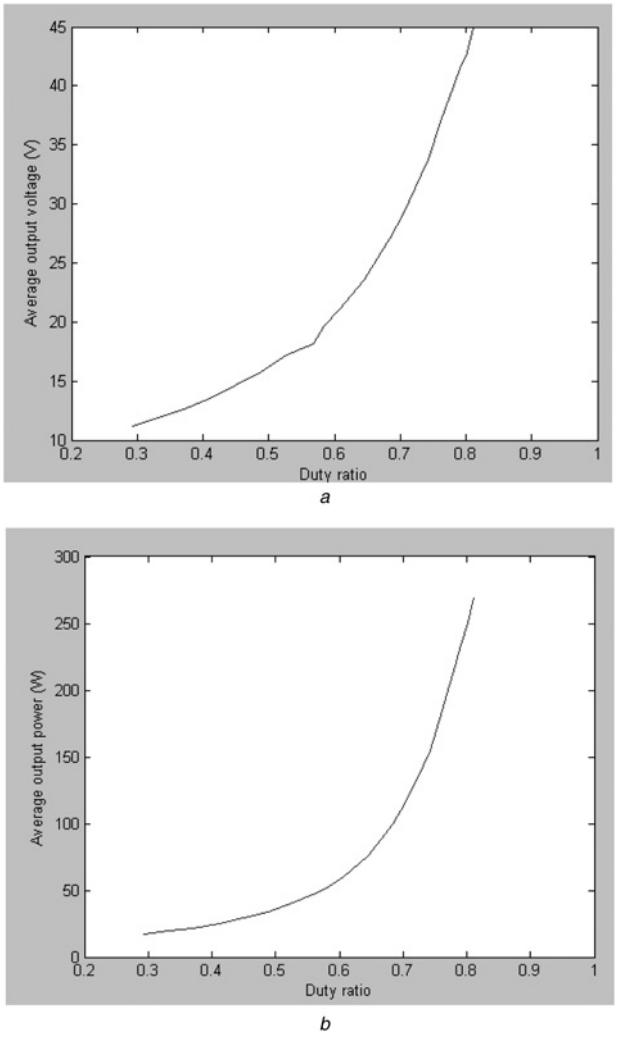


**Fig. 6** *Output characteristics*
*a* Average output voltage against $D^*$ curve
*b* Average output power against $D^*$ curve


© The Institution of Engineering and Technology 2012

doi: 10.1049/iet-pel.2012.0115

## 6 Experimental results of resistive load

Several tests were conducted on the test platform shown in Fig. 5 to compare the results under various operating conditions under constant and variable speed/load conditions using PWM and hysteresis current control methods as described below.

### 6.1 Test under constant speed and constant load

In this experiment, the test is carried out under constant speed and constant load and the output voltage is regulated by the following two methods.

1. Output voltage regulation through PWM controller (duty ratio, $D^*$):

Fig. 6*a* shows the average output voltage against $D^*$ curve obtained under constant speed (515 rpm) and constant load (7.55 Ω) conditions. Accordingly, average output power against $D^*$ curve is shown in Fig. 6*b*. A monotonic power curve with duty ratio can be seen. Figs. 7*a* and *b* show the waveforms of the phase current $I_{ph}$, the dc-link voltage $V_{dc}$ and the load current $I_L$ when $D^*$ is equal to 0.6.

2. Output voltage regulation through the current hysteresis control:

In this test, the output voltage is regulated by replacing the PWM controller with a hysteresis controller in Fig. 4 where it is shown that the magnitude of reference current $I_{ref}$ is modulated depending on the loading conditions so as to regulate the output voltage. Fig. 8*a* shows the average output voltage against $I_{ref}$ curve obtained under constant speed (515 rpm) and constant load (7.55 Ω) conditions. Accordingly the average output power against $I_{ref}$ curve is shown in Fig. 8*b*. It can be seen that a linear control of the power to current can be seen.

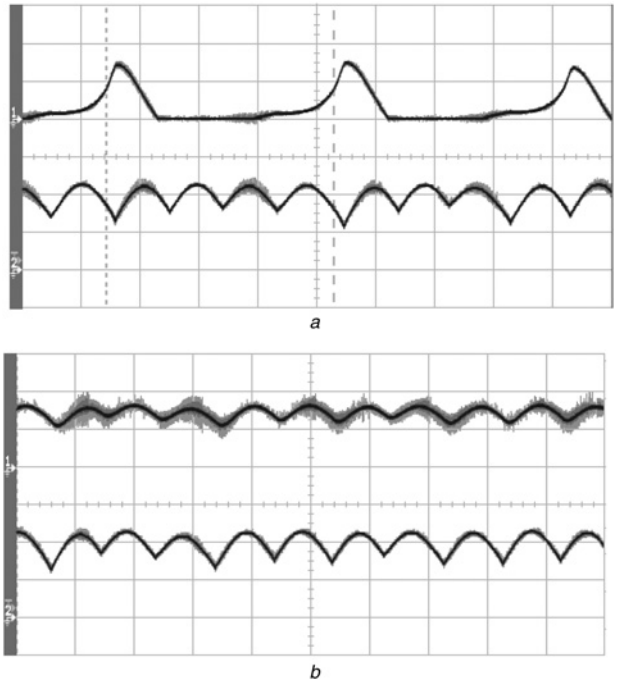

**Fig. 7** *Waveforms under resistive load and PWM control*

*a* Waveforms of $I_{ph}$ and $V_{dc}$ (Ch1: $I_{ph}$, 10 A/grid; Ch2: $V_{dc}$, 10 V/grid)
*b* Waveforms of $I_L$ and $V_{dc}$ (Ch1: $I_L$, 2 A/grid; Ch2: $V_{dc}$, 10 V/grid)

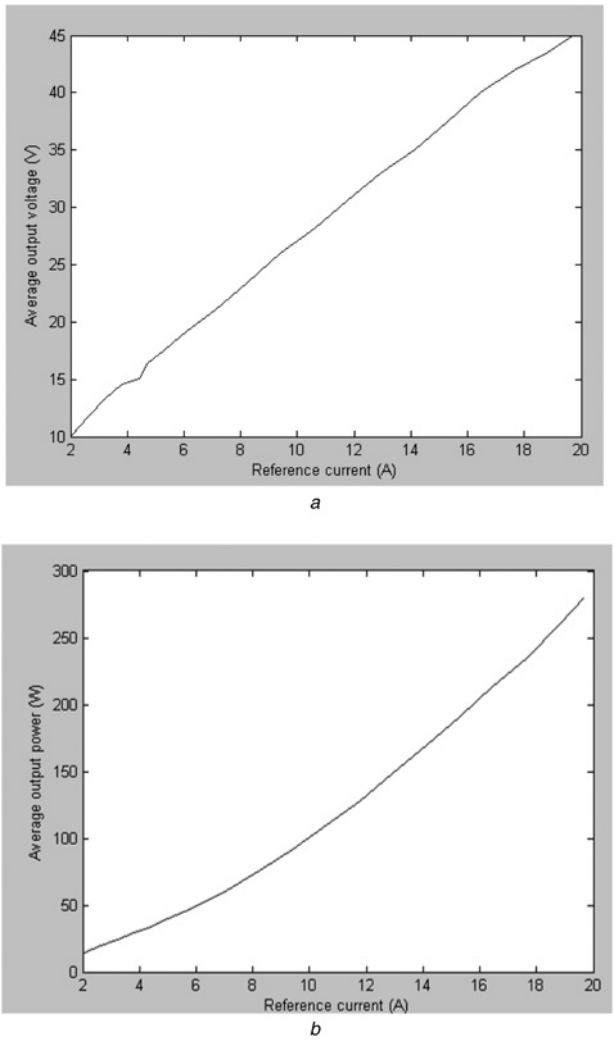


**Fig. 8** *Output characteristics*

*a* Average output voltage against $I_{ref}$ curve
*b* Average output power against $I_{ref}$ curve

In the hysteresis control method, two types of situations are encountered depending on the loading conditions under the same speed and $I_{ref}$ conditions. The results from the two situations are shown in Figs. 9*a* and *b*.

1. The light load (small $R$): $I_{ph}$ starts to increase since the two switches of the phase are closed at $\theta_{on}$. When $I_{ph}$ is equal to $I_{ref}$, the two switches of the phase are opened. Since the back emf is higher than the dc-link voltage at this moment, the current continues to increase. As a result, the hysteresis controller cannot regulate the current within the hysteresis band. The output of the hysteresis controller is therefore a single pulse as shown in Fig. 9*a*.
2. The high load (large $R$): $I_{ph}$ also starts to increase since the two switches of the phase are closed at $\theta_{on}$. When $I_{ph}$ is equal to $I_{ref}$, since the back emf is less than the dc-link voltage, the hysteresis controller will be able to regulate the current. The regulating action of the controller is depicted in the switching waveforms as shown in Fig. 9*b*.

### 6.2 Test under variable loads or variable speeds

According to the previous testing results (shown in Figs. 6 and 8) from different control methods under constant speed and



© The Institution of Engineering and Technology 2012

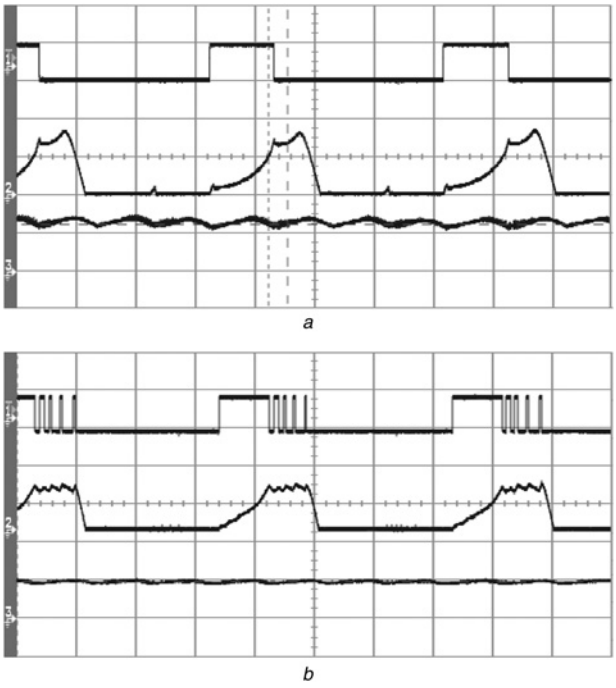

**Fig. 9** *Experimental waveforms using $I_{ref} = 7$ A hysteresis control and resistive load*

*a* Ch1: $PWM_{ph}$; Ch2: $I_{ph}$, 5 A/grid; Ch3: $V_{dc}$, 20 V/grid
*b* Ch1: $PWM_{ph}$; Ch2: $I_{ph}$, 5 A/grid; Ch3, 40 V/grid

constant load, it can be inferred that the hysteresis control method results in a linear relation between $I_{ref}$ and output voltage, whereas the PWM control results in a nonlinear relation between $D^*$ and output voltage. Hence, further experiments are carried out using the hysteresis control method.

Fig. 10*a* shows the waveforms of the dc-link voltage $V_{dc}$ and the phase current $I_{ph}$ when the step response of voltage reference $V_{dc}^*$ changes between 0 and 40 V (the resistive load: 36.07 Ω, speed: 563 rpm, PI controller: $P = 0.625$ and $I = 60$). $V_{dc}^*$ of I, II, III regions are of 0, 40 and 0 V, respectively. Fig. 10*b* shows the waveforms of the dc-link voltage $V_{dc}$ and the phase current $I_{ph}$ when the given resistive load is varied between 50 and 36.07 Ω ($V_{dc}^*$:32 V, speed: 515 rpm, PI controller: $P = 0.625$ and $I = 60$). The given resistive loads of Regions I, II, III are 50, 36.07 and 50 Ω, respectively.

The tests under variable given voltages, variable speeds and constant load are conducted (13 Ω) as well. The results of output power against different generator speeds are shown in Fig. 11. It is illustrated that good power control over a wide range of speed of generator using the proposed constant voltage control performance is achieved.

## 7 Experimental results of the battery pack paralleled a resistive load

Battery pack of 36 V, 55 Ah is used in the following tests and a resistor paralleled with the battery pack is used to mimic the load of the EV. In the following tests, the given voltage of SRG is constant 37 V and the speed is 995 rpm.

1. When the resistive load is open with ∞ Ω, the battery pack is charged with all the generated power: 69 W and the charging waveforms are shown in Fig. 12*a*.
2. When the resistance is 25 Ω, the battery pack is in mixed charging and discharging status. The waveforms are shown in

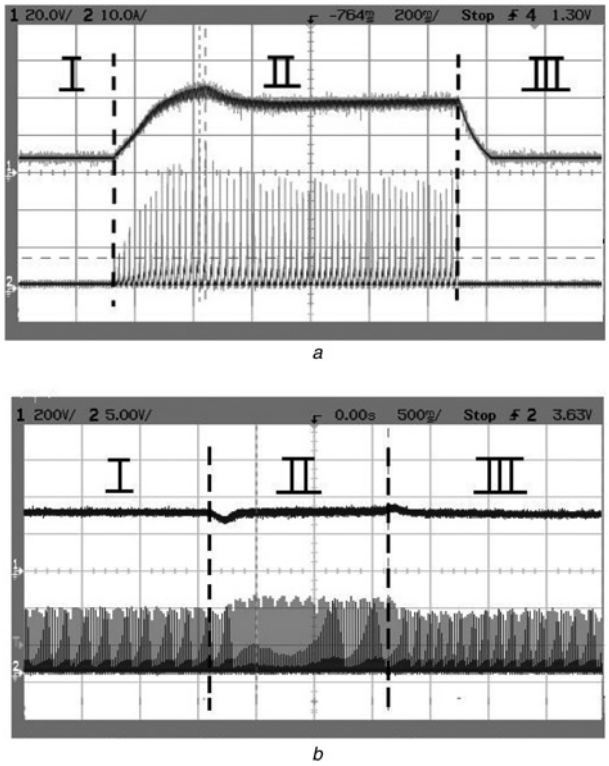

**Fig. 10** *Waveforms of $V_{dc}$ and $I_{ph}$ under variation of $V_{dc}^*$ and load*

*a* $V_{dc}^*$ changed between 0 and 40 V (Ch1: $V_{dc}$, 20 V/grid; Ch2: $I_{ph}$, 4 A/grid)
*b* Load changed between 50 and 36.07 Ω (Ch1: $V_{dc}$, 20 V/grid; Ch2: $I_{ph}$, 2 A/grid)

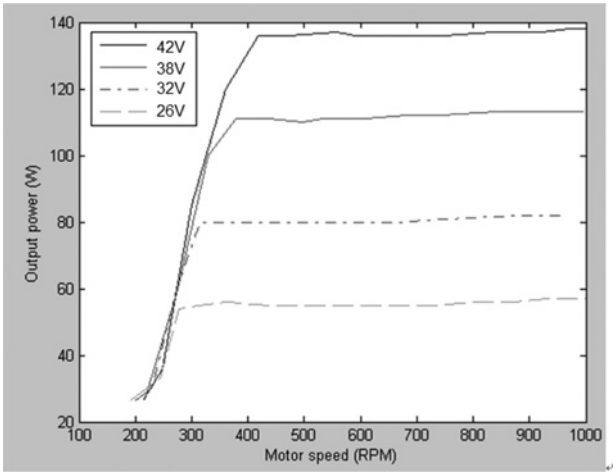


**Fig. 11** *Waveforms of output power against different motor speeds under the constant load resistance 13 Ω with various voltage commands*

Fig. 12*b* and the power consumed by the resistance and the generating power of the SRG are 55 and 69 W, respectively.
3. When the resistance is 10 Ω, the battery pack is in discharging status and the power consumed by the resistance is 129 W and it is larger than the generating power 69 W of SRG. Its waveforms are shown in Fig. 12*c*.
4. When the system is installed in a neighbourhood vehicle of 700 kg. The travelling distance is increased from 80 to 84 km per charge.

It can be concluded that SRG on-board generation system, connected to the battery pack paralleled with a resistive load,


© The Institution of Engineering and Technology 2012

doi: 10.1049/iet-pel.2012.0115

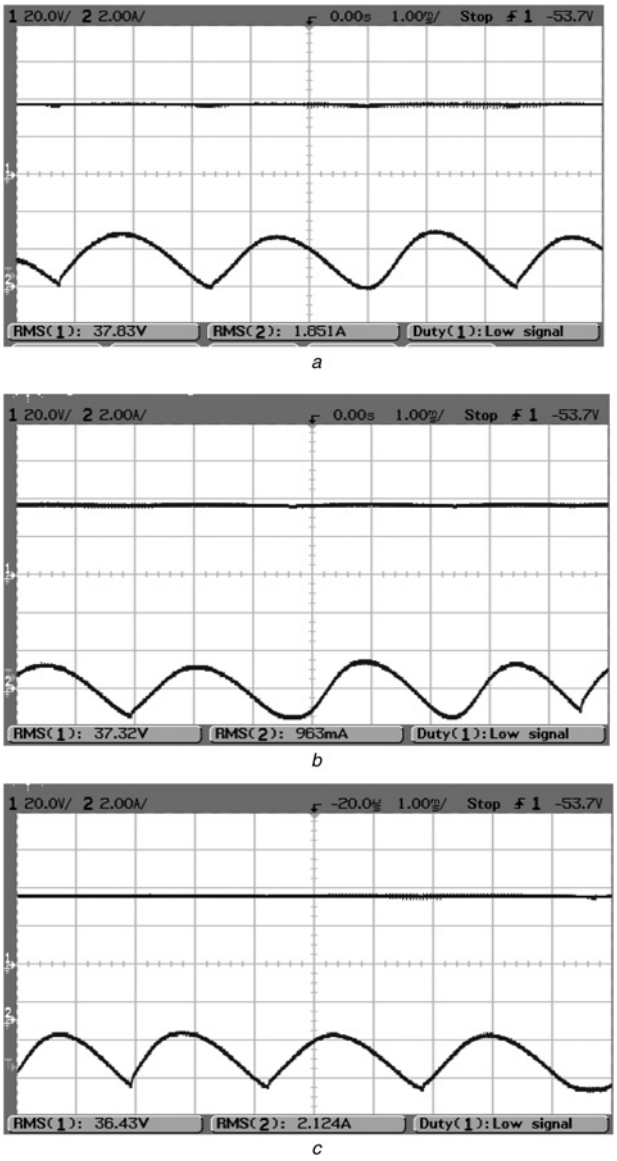


**Fig. 12** *Waveforms of $V_{dc}$ and $I_{Bat}$ with various loads (Ch1: $V_{dc}$, 20 V/grid; Ch2: $I_{Bat}$, 2 A/grid)*

*a* Battery pack only
*b* Battery pack paralleled with 25 Ω resistance
*c* Battery pack paralleled with 10 Ω resistance, and the speed is 995 rpm

can supply offset sinusoidal charging current for the battery pack and the load of the EV.

## 8 Conclusion

This paper has presented a testing platform for realising a new architecture for on-board power generation in a pure EV so as to extend the driving range. A new SRWPG system, as an important part of the new EV, has been investigated in this work. The development makes use of the wind power to form a structure in the vehicle to acquire additional power through a wind turbine. A new integrated wind turbine is proposed according to the requirements of the wind turbine for EVs. A new control scheme for an SRWPG system according to the operating conditions and characteristic of the wind power and SRGs is presented. Also, a control scheme for an SRG, as a part of the SRWPG system, is offered, and then different control strategies for an SRG are discussed. The various results from PWM and hysteresis control strategies are presented and compared, and the hysteresis control is selected as the preferred control because of the linear relationship between the output voltage and the hysteresis reference control parameter. The investigation into the realisation of on-board power generation with wind assisted SRG operation is very encouraging and provides good energy generation through on-board SRG on an EV.

## 9 Acknowledgment

The authors gratefully acknowledge the financial support from the Research Committee of the Hong Kong Polytechnic University for this project (Project no. 1-BB86).

## 10 References

1 Chan, C.C.: 'The state of the art of electric, hybrid, and fuel cell vehicles', *IEEE Proc.*, 2007, **95**, (4), pp. 704–718
2 Emadi, A., Williamson, S.S., Khaligh, A.: 'Power electronics intensive solutions for advanced electric, hybrid electric, and fuel cell vehicular power systems', *IEEE Trans. Power Electron.*, 2006, **21**, (3), pp. 567–577
3 Xue, X.D., Cheng, K.W.E., Sutanto, D.: 'Unified mathematical modelling of steady-state and dynamic voltage–current characteristics for PEM fuel cells', *Electrochim. Acta*, 2006, **52**, (3), pp. 1135–1144
4 Maberry, R.L.: 'Wind turbine driven generator system for a motor vehicle'. United States Patent, Patent No. US 7,147,069 B2, 2006
5 Liskey, K.W.: 'Airflow driven electrical generator for a moving vehicle'. United States Patent, Patent No. US 6,857,492, 2005
6 Chen, H., Gu, J.J.: 'Implementation of the three-phase switched reluctance machine system for motors and generators', *IEEE/ASME Trans. Mechatronics*, 2010, **15**, (3), pp. 421–432
7 Cardenas, R., Pena, R., Peraz, M., Clare, J., Asher, G., Wheeler, P.: 'Control of a switched reluctance generator for variable-speed wind energy applications', *IEEE Trans. Energy Convers.*, 2005, **20**, (4), pp. 781–791
8 Chang, Y.C., Liaw, C.M.: 'Establishment of a switched-reluctance generator-based common DC microgrid system', *IEEE Trans. Power Electron.*, 2011, **29**, (9), pp. 2512–2527
9 Shimizu, H., Harada, J., Bland, C., Kawakami, K., Chan, L.: 'Advanced concepts in electric vehicle design', *IEEE Trans. Ind. Electron.*, 1997, **44**, (1), pp. 14–18
10 Rajashekara, K., Fattic, J., Husted, H.: 'Comparative study of new on-board power generation technologies for automotive applications'. IEEE Workshop Power Electron. Transport., Auburn Hills, MI, 2002, pp. 3–10
11 Bao, Y.J., Cheng, K.W.E., Divakar, B.P.: 'Research on a novel switched reluctance wind power generator system for electric vehicles' (PESA, 2009), pp. 1–6
12 Kioskeridis, L., Mademlis, C.: 'Optimal efficiency control of switched reluctance generators', *IEEE Trans. Power Electron.*, 2006, **21**, (4), pp. 1062–1072
13 Wong, K.F., Cheng, K.W.E., Ho, S.L.: 'On-line Instantaneous torque control of switched reluctance motor based on co-energy control', *IET Proc., – EPA*, 2009, **3**, (4), pp. 257–264
14 Mademlis, C., Kioskeridis, I.: 'Optimizing performance in current-controlled switched reluctance generators', *IEEE Trans. Energy Convers.*, 2005, **20**, (3), pp. 556–565
15 Hayashi, Y., Miller, T.J.E.: 'A new approach to calculate core losses in the SRM', *IEEE. Trans. Ind. Appl.*, 1995, **31**, (5), pp. 1039–1046
16 Chang, Y.C., Liaw, C.M.: 'On the design of power circuit and control scheme for switched reluctance generator', *IEEE Trans. Power Electron.*, 2008, **23**, (1), pp. 445–454



© The Institution of Engineering and Technology 2012